# Improved Calibration Coefficients for *NOAA-12* and *NOAA-15* AVHRR Visible and Near-IR Channels

WILLIAM R. TAHNK AND JAMES A. COAKLEY JR.

*College of Oceanic and Atmospheric Sciences, Oregon State University, Corvallis, Oregon*

(Manuscript received 10 October 2001, in final form 6 March 2002)

ABSTRACT

A time history of the calibration coefficients for channels 1 and 2 of the Advanced Very High Resolution Radiometer (AVHRR) on the *NOAA-12* and *NOAA-15* spacecraft is presented. The history is based on reflectances observed for the interior zones of the Antarctic and Greenland ice sheets previously obtained with the *NOAA-9* AVHRR, which serves as the calibration standard. Reflectances observed in December and January for the Antarctic ice sheet are used to characterize sensor performance. Reflectances observed in May and June for the interior of the Greenland ice sheet are used to detect any substantial midyear shifts in the coefficients. Prelaunch calibration coefficients for the *NOAA-12* AVHRR are shown to be in error and the coefficients drift with time. The coefficients are compared with those reported in earlier studies, and the time rate of change of the calibration is found to be smaller than previously reported. The observations for the *NOAA-15* AVHRR are consistent with the prelaunch calibration coefficients for channel 1 but indicate a slight shift in the coefficients for channel 2. The calibration coefficients for the *NOAA-15* AVHRR appear to be stable. A slight drift in the response of channel 2 in the low-reflectance range is barely detectable.

## 1. Introduction

Measurements of reflected sunlight at a nominal wavelength of 0.64 $\mu$m, as observed with channel 1 of the National Oceanic and Atmospheric Administration (NOAA) Advanced Very High Resolution Radiometer (AVHRR), are used to retrieve properties of clouds (Han et al. 1994; Nakajima and Nakajima 1995; Wetzel and Stowe 1999). Combined with the channel 1 observations, measurements of reflected sunlight at a nominal wavelength of 0.84 $\mu$m, as observed with channel 2 of the NOAA AVHRRs, are used to retrieve properties of aerosols (Durkee et al. 1991; Higurashi and Nakajima 1999; Mischenko et al. 1999; Geogdzhayev et al. 2002; Coakley et al. 2002). Since the derived cloud and aerosol properties depend on the accuracy of the observed radiances, the radiometric drift of the AVHRR shortwave channels has received considerable attention. Rao and Chen (1995) provided a radiometric calibration for channels 1 and 2 of the *NOAA-9* AVHRR based on collocated observations made with calibrated aircraft radiometers. Using a portion of the Lybian desert, they transferred the calibration for the *NOAA-9* AVHRR to the *NOAA-7* and *NOAA-11* AVHRRs. They also used the desert to extend the calibration to the *NOAA-14* AVHRR (Rao and Chen 1996). Loeb (1997) used the radiometric calibration of the *NOAA-9* AVHRR and developed standard channel-1 and channel-2 reflectances for the interior ice sheets of Antarctica and Greenland. He showed that these standard reflectances were stable for 1985 and 1986. He then used the ice sheets to check and extend the calibration of channels 1 and 2 for the *NOAA-11*, *-12*, and *-14* AVHRRs. Brest et al. (1997) used the *NOAA-9* AVHRR to develop a global climatology of cloud-free channel-1 reflectances. They then used monthly mean averages of the departures of cloud-free reflectances from the climatological values to derive calibration coefficients for AVHRR channel 1 on the *NOAA-7, -8, -10, -11,* and *-12* spacecraft. Tahnk and Coakley (2001a,b) used the Antarctic and Greenland ice sheets to extend the record started by Loeb (1997) for the *NOAA-14* AVHRR. Masonis and Warren (2001) also used the Antarctic and Greenland ice sheets to establish records of drift for channels 1 and 2 of the *NOAA-9, -10,* and *-11* AVHRRs. Here, the Antarctic and Greenland ice sheets are used to establish the time history of the calibration for channels 1 and 2 of the *NOAA-12* and *NOAA-15* AVHRRs. In the case of the *NOAA-12* AVHRR, the time history derived here is consistent with the assessment made by Loeb (1997). For channel 1, the reflectances calculated here for the beginning of the *NOAA-12* AVHRR are 7% smaller and the time rate of change of the reflectances are considerably smaller than the values given by Brest et al. (1997). While details of the der-

*Corresponding author address:* James A. Coakley Jr., College of Oceanic and Atmospheric Sciences, Ocean Admin. 104, Oregon State University, Corvallis, OR 97331-5503.
E-mail: coakley@coas.oregonstate.edu

ivation of the coefficients are given in Loeb (1997) and in Tahnk and Coakley (2001a), a brief description of the approach is provided here.

## 2. Analysis

The reflectance measured in an AVHRR field of view is represented by a 10-bit raw pixel count. The reflectance for channel $i$ is given by

$$R_i = \frac{r_i \delta_{ES}}{\mu_0} \tag{1}$$

with $r_i = \alpha_i C_{10}^i - \beta_i$, where

$R_i$ = reflectance (equivalently, the isotropic albedo in %),
$r_i$ = instrument reflectance (%),
$\alpha_i$ = slope (% reflectance/count),
$C_{10}^i$ = 10-bit raw pixel count,
$\beta_i$ = offset (% reflectance),
$\delta_{ES}$ = correction for mean Earth–Sun distance,
$\mu_0$ = $\cos\theta_0$ with $\theta_0$ the solar zenith angle.

A distinction is made between $R_i$, which represents the reflectance for the individual observation and is a physical quantity, and $r_i$, which is proportional to the radiance measured by the AVHRR, and referred to as ''albedo'' in the NOAA *Polar Orbiter User's Guide* (Kidwell 1994). Here $r_i$ is referred to as ''instrument reflectance.''

Using the calibration of the *NOAA-9* AVHRR based on aircraft observations (Rao and Chen 1995), Loeb (1997) showed that for the interior ice sheets, spatially uniform targets observed near nadir had channel-1 and -2 reflectances given by

$$R_1 = 74.25 + 0.8953\theta_0 - 0.01233\theta_0^2 \tag{2a}$$

$$R_2 = 60.29 + 0.8305\theta_0 - 0.00915\theta_0^2 \tag{2b}$$

for Antarctica in December, and by

$$R_1 = 81.37 + 0.5202\theta_0 - 0.009152\theta_0^2 \tag{3a}$$

$$R_2 = 103.9 - 0.6072\theta_0 + 0.001373\theta_0^2 \tag{3b}$$

for Greenland in June. The reflectances in (2) are restricted to solar zenith angles between 63° and 80°; those in (3) are restricted to solar zenith angles between 46° and 73°. Loeb (1997) demonstrated that (2) and (3) were repeatable for 1985 and 1986. For the channel-1 observations of Greenland, Tahnk and Coakley (2001a) found the reflectance standards proposed by Loeb (1997) to be satisfactory for May and June. For channel 2, on the other hand, they proposed a new reflectance standard for the Greenland ice sheet based on reflectances observed with the *NOAA-14* AVHRR at solar zenith angles not analyzed by Loeb (1997). In applying this new standard to *NOAA-12* and *NOAA-15* observations, however, reflectances observed in both channels 1 and 2 for July and August fell markedly below the reflectances observed in May and June of the same year and for the same solar zenith angles. The smaller reflectances observed for late summer may well have been caused by extensive meltwater (Stroeve et al. 1997). In addition, Masonis and Warren (2001) note that day-to-day changes in surface grain size of snow affects the reflectances in the near infrared more so than at visible wavelengths. Changes in the grain size of the snow may also contribute to the relatively large variability of the channel-2 reflectances. For these reasons, the channel-2 observations of Greenland were restricted to June and the standard reflectances proposed by Loeb (1997) were used. Because the observations for Greenland exhibit larger variability than those for Antarctica, perhaps in part due to meltwater and rapid changes in the surface grain size, the observations of the Antarctic ice sheet are used to derive calibration coefficients while observations of the Greenland ice sheet serve as a midyear check for any substantial changes in the coefficients. Such a check may prove useful as significant changes, even in sign, have been reported for the time-rate of change of the calibration coefficients for the *NOAA-10* and *NOAA-14* AVHRRs (Tahnk and Coakley 2001b; Masonis and Warren 2001).

For *NOAA-12,* launched in May 1991, daily AVHRR Global Area Coverage (GAC) (Kidwell 1994) observations were analyzed for the months of January 1992–98 and December 1998 for Antarctica, and for May and June 1992–98 for Greenland. Owing to a failure in the onboard GAC recorder, and the lack of data from a High Resolution Picture Transmission (HRPT) receiving station for either region, *NOAA-12* AVHRR GAC and HRPT data are unavailable for Antarctica and Greenland after December 1998. For *NOAA-15,* launched in May 1998, daily GAC observations were analyzed for December 1998, 1999, and 2001 and January 1999, 2000, and 2002 for Antarctica and May and June 1999–2001 for Greenland. As explained later, the *NOAA-15* AVHRR has two instrument slopes to be determined for both channel 1 and channel 2: one for low ranges of reflectances and a second for high ranges. The observations of Antarctica permitted only the calibration of the low-range reflectances. In addition, owing to a failure in the AVHRR scanning motor, *NOAA-15* AVHRR data are unavailable between November 2000 and March 2001.

The standard reflectances that Loeb (1997) established for the Antarctic ice sheet were based solely on December observations. Here we use January observations of Antarctica from the *NOAA-12* AVHRR and December and January observations from the *NOAA-15* AVHRR. The *NOAA-15* observations for both December and January fit the standard reflectances equally well, suggesting that the standard reflectances for Antarctica are applicable for both December and January observations.

Following Loeb (1997), the satellite observations used to derive calibration coefficients are restricted to nadir

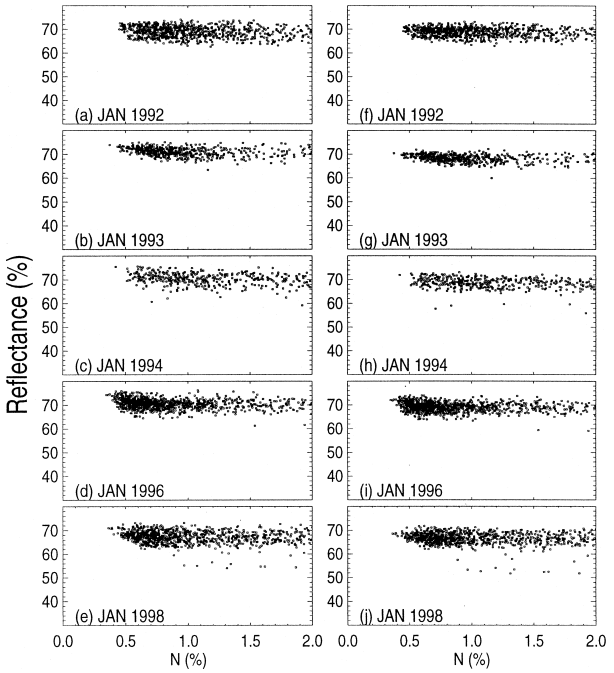


FIG. 1. *NOAA-12* AVHRR reflectances for Antarctica and *N*, the spatial uniformity index, for 17 × 17 arrays of 4-km pixels with view zenith angles less than 18° and solar zenith angles between 75° and 80° for (a)–(e) channel 1 and (f)–(j) channel 2. The reflectances were obtained using the prelaunch calibration of the instrument reflectances given by (5a) and (5b).

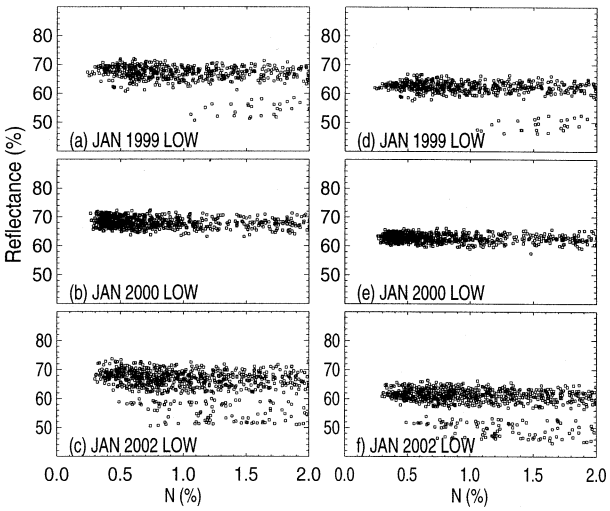


FIG. 2. *NOAA-15* AVHRR reflectances for Antarctica and *N*, the spatial uniformity index, for 17 × 17 arrays of 4-km pixels with view zenith angles less than 18° and solar zenith angles between 75° and 80° for (a)–(c) channel 1 and (d)–(f) channel 2. Low-range instrument reflectances were used for both channels. The reflectances were obtained using the prelaunch instrument reflectances given by (6a) and (6c).

observations (view zenith angles less than 18°) and subjected to a spatial uniformity test. By restricting the observations to near nadir viewing geometries, effects due to the anisotropy of the reflected radiances are reduced. For the spatial uniformity test, the GAC AVHRR 4-km data are divided into 17 scan line by 17 scan spot scenes covering approximately (68 km)$^2$ subregions at nadir. Large spatial variations are avoided by selecting these scenes to be away from coastal regions and well within the interiors of the continents. For Antarctica, scenes were collected for 72°–80°S and 90°–130°E. For Greenland, scenes were collected for 73°–78°N and 32°–48°W. An index of spatial uniformity is calculated for each (68 km)$^2$ scene. The index is given by

$$N = \frac{1}{4}\left(\frac{\sigma_1}{\overline{R_1}} + \frac{\sigma_2}{\overline{R_2}} + \frac{\sigma_3}{\overline{T_3}} + \frac{\sigma_4}{\overline{T_4}}\right) \times 100\%, \qquad (4)$$

where (for channel number given by the subscript):

$N$ = index of spatial uniformity (in %),
$\overline{R_1}$, $\overline{R_2}$ = mean channel reflectances,
$\sigma_1$, $\sigma_2$ = standard deviation of channel reflectances,
$\overline{T_3}$, $\overline{T_4}$ = mean channel brightness temperatures,
$\sigma_3$, $\sigma_4$ = standard deviation of channel brightness temperatures.

Small *N* implies spatial uniformity in reflectances and brightness temperatures within the scene. Spatial uniformity is obviously desirable in a calibration target. Any spatial variability could be caused by clouds or by spatial variability in the snow and ice surfaces. As was pointed out by Loeb (1997), cloud particles scatter strongly in the forward direction. Consequently, when the incident sunlight is at high solar zenith angles, as it is for the observations of Antarctica and Greenland, scenes with highly reflecting surfaces, like snow and ice, have lower nadir reflectances when overcast than when cloudfree. The forward scattering by the cloud particles directs the incident sunlight away from the surface so that the light cannot be redirected by the surface toward the nadir-viewing satellite radiometer. In other words, clouds increase *N* and lower the nadir reflectance. As illustrated in the next section, $N < 0.5\%$ appears to remove contamination by objects that would reduce the observed reflectances.

## 3. Results

Figures 1 and 2 show reflectances and *N*, the index of spatial uniformity, for *NOAA-12* and *NOAA-15* AVHRR channels 1 and 2. Because the observations are consistent with those of the other years, the *NOAA-12* AVHRR observations for January 1995 and January 1997 are not shown. For consistency between years, only subregions with solar zenith angles between 75° and 80° are shown for both *NOAA-12* and *NOAA-15*. The reflectances in the figures were calibrated using the prelaunch calibration coefficients supplied by NOAA National Environmental Satellite Data and Information Service (Kidwell 1994) and imbedded in the level 1b

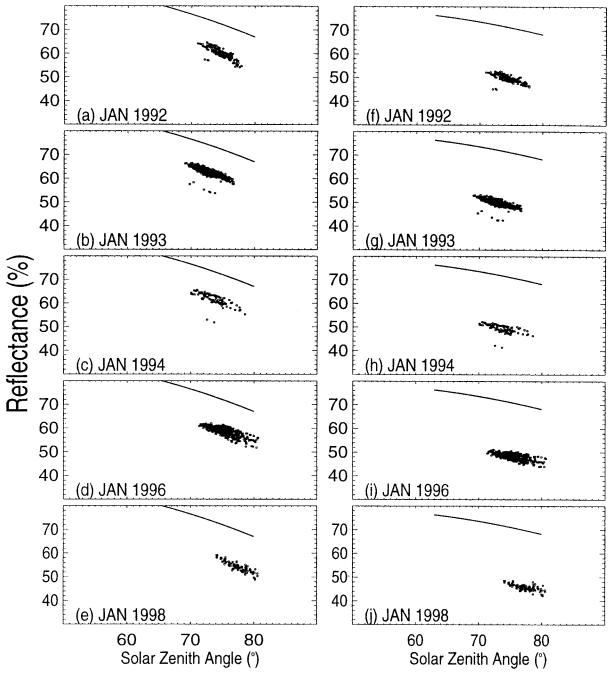


FIG. 3. *NOAA-12* AVHRR reflectances for Antarctica and solar zenith angles for 17 × 17 arrays of 4-km pixels with spatial uniformity index, $N < 0.5\%$ for (a)–(e) channel 1 and (f)–(j) channel 2. The solid lines represent the *NOAA-9* calibration references for Antarctica as given by (2a) and (2b). The *NOAA-12* reflectances were obtained using the prelaunch instrument reflectances given by (5a) and (5b).

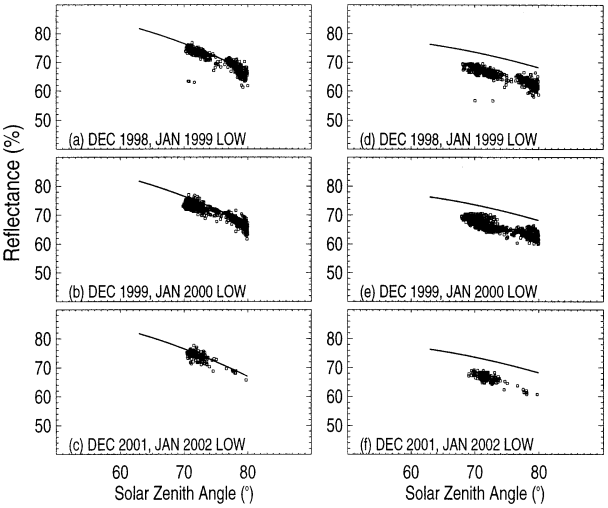


FIG. 4. *NOAA-15* AVHRR reflectances for Antarctica and solar zenith angles for 17 × 17 arrays of 4-km pixels with spatial uniformity index, $N < 0.5\%$ for (a)–(c) channel 1 and (d)–(f) channel 2. Low-range instrument reflectances were used for both channels. The solid lines represent the *NOAA-9* calibration references for Antarctica as given by (2a) and (2b). The *NOAA-15* reflectances were obtained using the prelaunch instrument reflectances given by (6a) and (6c).

data. For *NOAA-12*, the channel-1 and -2 instrument reflectances are given by

$$r_1 = 0.1042C_{10}^1 - 4.4491 \quad (5a)$$

$$r_2 = 0.1014C_{10}^2 - 3.9926. \quad (5b)$$

The *NOAA-15* AVHRR has a dual slope gain function for the visible and near-IR channels. The augmented gain enhances radiometric resolution at low values of the instrument reflectances, with only minor loss of resolution at higher values of the instrument reflectances. For channel 1, the *NOAA-15* AVHRR prelaunch instrument reflectances are given by

$$r_1^{\mathrm{LOW}} = 0.0568C_{10}^1 - 2.1874 \quad (6a)$$

$$r_1^{\mathrm{HIGH}} = 0.1633C_{10}^1 - 54.9928, \quad (6b)$$

with a transition pixel count of 496. For channel 2 the reflectances are given by

$$r_2^{\mathrm{LOW}} = 0.0596C_{10}^2 - 2.4096 \quad (6c)$$

$$r_2^{\mathrm{HIGH}} = 0.1629C_{10}^2 - 55.2436, \quad (6d)$$

with a transition pixel count of 511.

As shown in Figs. 1 and 2, for all years and both channels, when $N \leq 0.5\%$, the reflectances are tightly clustered. As $N$ becomes large, so that the reflected and emitted radiances acquire spatial variability, the reflectances become scattered and the mean of the reflectances for a particular value of $N$ is depressed below the values obtained for $N \leq 0.5\%$. As was noted earlier, for nadir views and high solar zenith angles, the forward scattering of sunlight by clouds prevents the incident light from reaching the surface, thereby reducing the nadir reflectance. The scattered points with $N > 0.5\%$ and reflectances falling beneath the main population of points for *NOAA-12* (Fig. 1) and *NOAA-15* (Fig. 2) are probably due to clouds. In the case of the January 2002 *NOAA-15* observations, the points in the branch with lower reflectances also have large reflectances at 3.7 $\mu$m (not shown). These large 3.7-$\mu$m reflectances are probably due to small droplets or ice crystals in clouds. Cloud-free snow and ice scenes ($N \leq 0.5\%$) have relatively small reflectances at 3.7 $\mu$m.

Figures 3 and 4 show *NOAA-12* and *NOAA-15* reflectances for channels 1 and 2 as a function of solar zenith angle for only those Antarctic subregions that displayed a high degree of spatial uniformity ($N < 0.5\%$). Superimposed on the observations are the standard reflectances derived from *NOAA-9* observations (2a and 2b). For *NOAA-12* (Fig. 3), reflectances are poorly calibrated from the start and the departures of the reflectances from the standard reflectances varies with year. The poor calibration at launch undoubtedly resulted from the many years (approximately a decade) between the completion of prelaunch calibration and the launch of the satellite. For *NOAA-15* (Fig. 4), reflectances appear to be well calibrated in channel 1 but there is a slight shift in the calibration of the reflectances for channel 2. Changes of the *NOAA-15* AVHRR calibration coefficients with time are hard to detect in either chan-

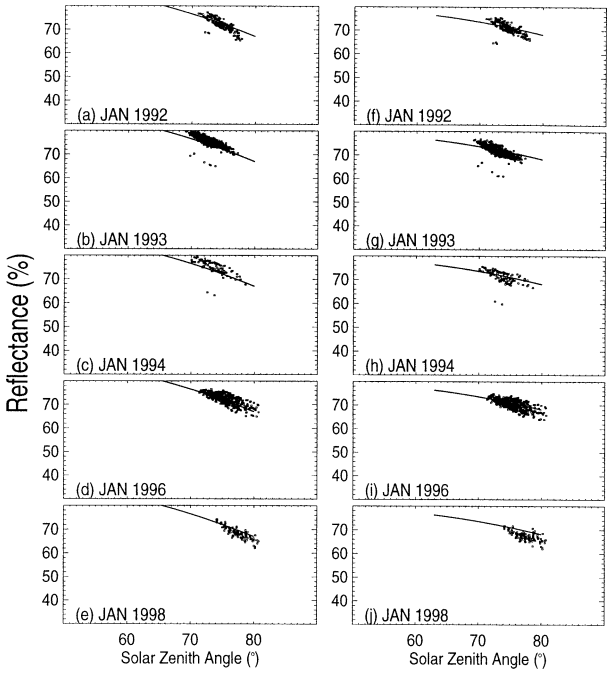


FIG. 5. Same as Fig. 3 but the *NOAA-12* reflectances were obtained using the instrument reflectances given by (7a) and (7b).

nel. Figure 4 shows that the *NOAA-15* AVHRR reflectances for December and January fit the standard reflectances equally well suggesting that the standard reflectances for Antarctica are applicable for both months.

New calibration coefficients were developed for *NOAA-12* and *NOAA-15* using the *NOAA-9* reflectances for Antarctica given by (2a) and (2b). Based on observed AVHRR reflectances for January 1994–98, the new *NOAA-12* coefficients are given by

$$r_1 = [(3.7 \pm 0.4) \times 10^{-6} d + (0.121 \pm 0.002)] \times (C_{10}^1 - C_0^1) \quad (7a)$$

$$r_2 = [(3.2 \pm 0.5) \times 10^{-6} d + (0.143 \pm 0.002)] \times (C_{10}^2 - C_0^2), \quad (7b)$$

where $d$ = day since launch (14 May 1991: $d = 0$) and average values are used for the deep space counts, $C_0^1 = 40.3$ and $C_0^2 = 40.0$ (Mitchell 1999). The values used for the deep space counts differ slightly from those inferred from the prelaunch slope and offset given by (5a) and (5b), $C_0^1 = 42.7$, and $C_0^2 = 39.4$.

Using AVHRR reflectances for Antarctica for December 1998, 1999, and 2001 and January 1999, 2000, and 2002, the derived *NOAA-15* coefficients for low-range reflectances are given by

$$r_1 = [(-0.1 \pm 0.3) \times 10^{-6} d + (0.058 \pm 0.002)] \times (C_{10}^1 - C_0^1) \quad (8a)$$

$$r_2 = [(0.8 \pm 0.4) \times 10^{-6} d + (0.065 \pm 0.002)] \times (C_{10}^2 - C_0^2), \quad (8b)$$

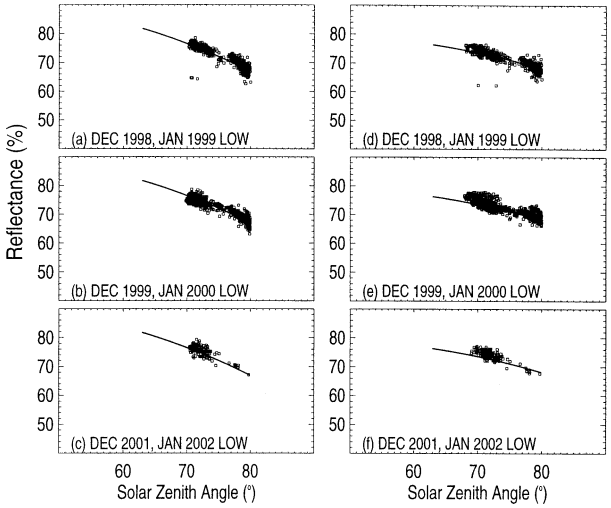


FIG. 6. Same as Fig. 4 but the *NOAA-15* reflectances were obtained using the low-range instrument reflectances given by (8a) and (8b).

where $d$ = day since launch (13 May 1998: $d = 0$) and the deep space count for channel 1 is taken to be $C_0^1 = 38$ and that for channel 2, $C_0^2$, switches between 38 and 39 as given in the level 1b data. These values differ slightly from the prelaunch values inferred from (6a) and (6c), $C_0^1 = 38.5$ and $C_0^2 = 40.4$. Unfortunately, owing to the low levels of incident sunlight for Antarctica, no assessment of the calibration could be made for the high instrument reflectance range. Since instrument gain is changed at count 496 for channel 1 and 511 for channel 2, there appears to be no way of matching the radiometric calibration given by (8a) and (8b) to the high instrument reflectance ranges unless the calibrations for the high instrument reflection ranges have undergone corresponding changes.

Figures 5 and 6 are identical to Figs. 3 and 4, except that the *NOAA-12* reflectances (Fig. 5) are obtained using (7a) and (7b), and the *NOAA-15* reflectances are obtained using (8a) and (8b) for the low-range instrument reflectances. The reflectances for $N < 0.5\%$ are consistent with those derived from *NOAA-9* AVHRR (the solid lines in Figs. 5 and 6). For January 1992 and 1993 (Figs. 5a, 5b, 5f, and 5g), the slope of the reflectance as a function of the solar zenith angle for *NOAA-12* is inconsistent with slope derived from the *NOAA-9* observations for channels 1 and 2. The inconsistency may be a consequence of the stratospheric aerosol layer that formed after the June 1991 eruption of Mt. Pinatubo. The results of radiative transfer calculations suggest that as in the case of clouds when the solar zenith angle is large, forward scattering by the aerosol prevents a sufficient amount of radiation from reaching the surface and being reflected in the nadir direction. The reduction in scene reflectance due to the presence of the aerosol becomes larger as the solar zenith angle increases. This behavior is consistent with the slopes of the reflectance as a function of solar zenith angle for the observations being larger in 1992 and 1993

than the slopes given by the standard reflectances as given by the solid lines in the figure. The reflectances beginning with January 1994 appear to be consistent with the *NOAA-9* standard. Although the results in Fig. 5 suggest that the stratospheric aerosol has little effect on the magnitude of the observed mean reflectance, radiative transfer calculations suggest that the reflectances with the stratospheric aerosol should reduce the scene reflectance as was reported for channel 1 of the *NOAA-11* AVHRR (Masonis and Warren 2001). As a result, the January 1992 and 1993 *NOAA-12* observations were not used to derive (7a) and (7b), thereby minimizing any possible influence from the Mt. Pinatubo eruption.

Figures 7 and 8 show the change in the count-to-reflectance slope with time for channel-1 and -2 reflectances, superimposed on the slopes given in (7a) and (7b) (solid lines) for *NOAA-12* (Fig. 7) and in (8a) and (8b) for *NOAA-15* low-range reflectance observations (Fig. 8). Each point in the figure represents the mean of the slopes calculated on a particular day, either for Antarctica (January 1992–98 and December 1998 for *NOAA-12* and December 1998, 1999, and 2001 and January 1999, 2000, and 2002 for *NOAA-15*) or for Greenland (May and June for channel 1 and June for channel 2 for 1993, 1995, and 1997 *NOAA-12* observations and for 1999–2001 *NOAA-15* observations). The considerable spread in the values and the significant departures for most of the June channel-2 slopes from the predicted values illustrates the caution voiced by Masonis and Warren (2001) that owing to the dependence of the near-infrared reflectance on surface grain size, snow surfaces may not be suitable for calibration targets.

The *NOAA-12* observations of Antarctica fit the count to reflectance slope, $\alpha_i$ in (1), as given in (7a) and (7b) with an rms uncertainty of 2% for channel 1 and 1% for channel 2. The absolute accuracy of the calibration is ~5%, the accuracy given by Loeb (1997) for the standard reflectances. The channel-1 and channel-2 slopes for January 1995 and 1996 agree with the values given by Loeb (1997) for December 1994 and 1995 within the 5% absolute uncertainty ascribed to the coefficients. According to Loeb (1997), from December 1994 to December 1995, the slopes changed by approximately 2% in both channels, compared with 1% for channel 1 and 0.8% for channel 2 in the current study. The annual rate of change in the slope for channel 1 given by Brest et al. (1997) is much higher, 5%. Such a high rate of change in the slope is not supported by the observations presented here. In addition, Brest et al. (1997) use 0.908 as the ratio between the calibrated *NOAA-9* AVHRR channel-1 reflectances and the *NOAA-12* AVHRR reflectances at launch. Here from (5a) and (7a) the ratio is $0.104/(0.121 \pm 0.002) = 0.86 \pm 0.02$. While this difference is bridged by the uncertainties, 5% as given here and 10% as given by Brest et al. (1997) for the absolute calibration, owing to the large difference in the time-rate of change, differences in the channel-1 calibration grow with time so that by the end of the record in December 1998, the predicted channel-1 reflectances will depart by more than 30%.

Interestingly, the channel-1 slope for June of 1992 falls well below the values given by (6a), and the channel-1 slope for June 1993 also is somewhat below the expected value. There appears to be no corresponding drop in the slopes estimated for channel 2. The drop in the slope for channel 1 indicates that the reflectance for the Greenland ice sheet was unusually large for June 1992 and somewhat so for 1993 while it remained relatively constant in other years. Based on the results of radiative transfer calculations a large reflectance in channel 1 with no discernible change in channel 2 is not likely to be due to an aerosol layer. The behavior would be consistent with low values of stratospheric ozone for June 1992, but the reduction required to achieve the ~6% reduction in slope is ~50% of the column ozone. Consequently, no explanation other than measurement uncertainty can be offered for the low values of the channel-1 slopes deduced from observations of the Greenland ice sheet in June of 1992 and 1993. While the 1992 and 1993 observations for Antarctica were not used to develop (7a) and (7b), the departure of the channel slopes from the predicted values for those years is small, indicating that the Mt. Pinatubo eruption had little effect on the radiometric stability of the Antarctic ice sheet.

For *NOAA-15,* the observations of Antarctica fit the count to reflectance slope given by (8a) and (8b) with an rms uncertainty of 3% for both channels. Again, owing to the uncertainty in the reflectance standard, the absolute accuracy is ~5%. For channel 1, the slope differs little from the prelaunch value given in (6a). For channel 2, the departure of the slope from the prelaunch value in (6c) is small but appears to be significant. As (8a) and (8b) indicate, and as is illustrated in Fig. 8, there appears to be no significant change in the slopes with time.

## 4. Summary and conclusions

Analyses of cloud-free *NOAA-12* and *NOAA-15* channel-1 and -2 reflectances for the interior ice sheets of Antarctica and Greenland were conducted in order to evaluate the accuracy of the prelaunch calibration coefficients. Based on *NOAA-12* data from January 1994–98 and December 1998 for Antarctica, the prelaunch coefficients (5a) and (5b) for deriving reflectances for the *NOAA-12* AVHRR visible and near-IR bands are in error. Consequently, revised calibration coefficients were developed (7a and 7b). The revised coefficients yield *NOAA-12* AVHRR reflectances that are stable for the 7-yr period. Based on *NOAA-15* AVHRR data from December 1998, 1999, and 2001 and January 1999, 2000, and 2002 for Antarctica, low-range reflectance observations were well calibrated in channel 1 but not in channel 2, using prelaunch coefficients (6a) and (6c). A revised set of calibration coefficients was developed

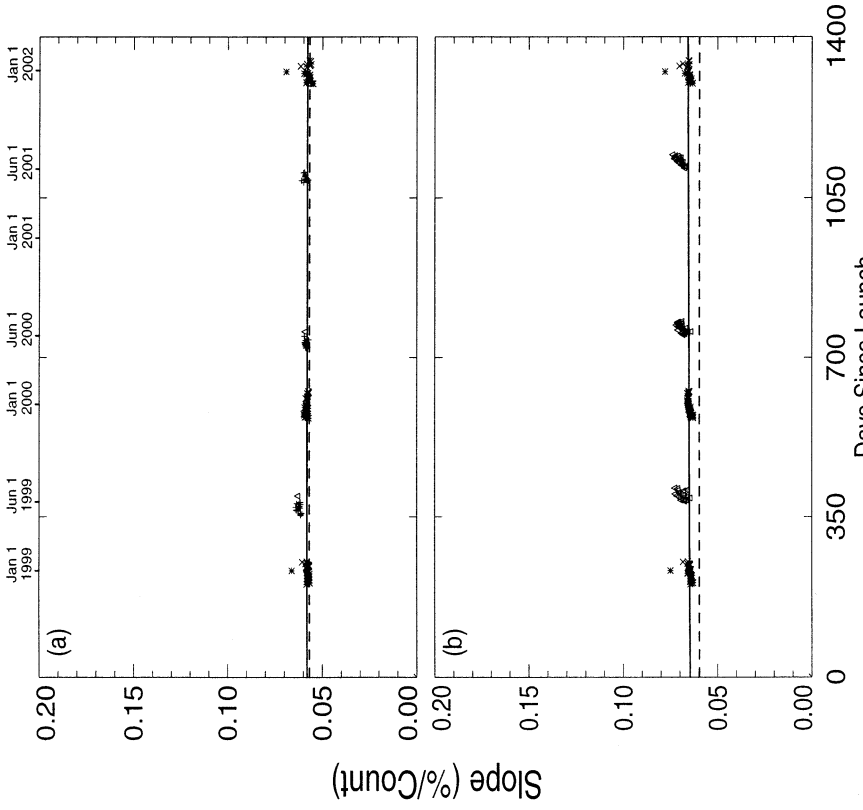


FIG. 8. Count-to-reflectance slope for (a) channel 1 and (b) channel 2 of the *NOAA-15* AVHRR for the low-range of instrument reflectances. Plotted symbols represent daily mean slopes for *NOAA-15* passes from May (+) and Jun (Δ) over Greenland for 1999–2001 and from Dec (*) 1998, 1999, and 2001 and Jan (×) 1999, 2000, and 2002 over Antarctica. The solid lines are the slopes given in (8a) and (8b) and the dashed lines are the prelaunch slopes given in (6a) and (6c).

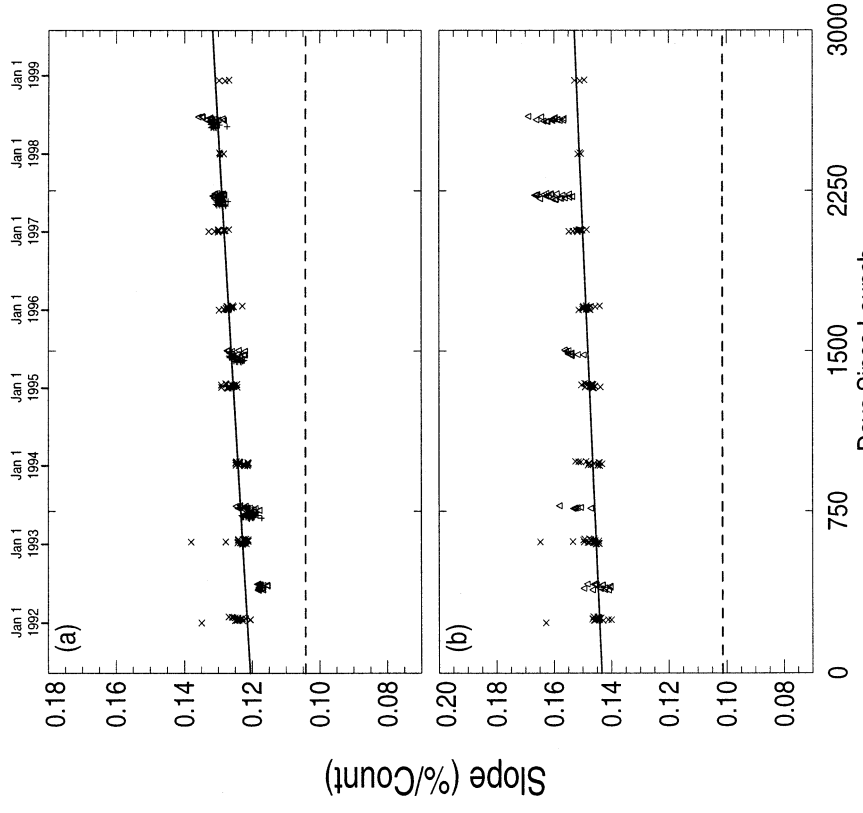


FIG. 7. Count-to-reflectance slope for (a) channel 1 and (b) channel 2 of the *NOAA-12* AVHRR. Plotted symbols represent daily mean slopes for *NOAA-12* passes from May (+) and Jun (Δ) over Greenland for 1993, 1995, and 1998, and from Jan (×) 1992–98 and Dec 1998 over Antarctica. The solid lines are the slopes given in (7a) and (7b) and the dashed lines are the prelaunch slopes given in (5a) and (5b).

for the *NOAA-15* AVHRR (8a and 8b). In addition, the calibration of the *NOAA-15* AVHRR was shown to be stable for the 3 yr examined here.

*Acknowledgments.* This work was supported in part by the National Science Foundation (NSF), ATM-9612886, the Center for Clouds, Chemistry, and Climate at the Scripps Institute of Oceanography, an NSF Science and Technology Center, and the Global Aerosol Climatology Project through NASA Grant NAG5-7686.

## REFERENCES

Brest, C. L., W. B. Rossow, and M. D. Roiter, 1997: Update of radiance calibration for ISCCP. *J. Atmos. Oceanic Technol.,* **14,** 1091–1109.

Coakley, J. A., Jr., W. R. Tahnk, C. Devaux, A. Jayaraman, P. K. Quinn, and D. Tanré, 2002: Aerosol optical depth and direct radiative forcing for INDOEX derived from AVHRR: Theory. *J. Geophys. Res.*, in press.

Durkee, P., F. Pfeil, E. Frost, and E. Shima, 1991: Global analysis of aerosol particle characteristics. *Atmos. Environ.,* **25A,** 2457–2471.

Geogdzhayev, I. V., M. I. Mishchenko, W. B. Rossow, B. Cairns, and A. A. Lacis, 2002: Global two-channel AVHRR retrievals of aerosol properties over the ocean for the period of *NOAA-9* observations and preliminary retrievals using *NOAA-7* and *NOAA-11* data. *J. Atmos. Sci.,* **59,** 262–278.

Han, Q., W. B. Rossow, and A. A. Lacis, 1994: Near-global survey of effective droplet radii in liquid water clouds using ISCCP data. *J. Climate,* **7,** 465–497.

Higurashi, A., and T. Nakajima, 1999: Development of a two channel aerosol retrieval algorithm on global scale using NOAA AVHRR. *J. Atmos. Sci.,* **56,** 924–941.

Kidwell, K. B., 1994: *NOAA Polar Orbiter Users Guide.* U.S. Department of Commerce, NOAA, NESDIS, NCDC, Satellite Data Services Division, 410 pp.

Loeb, N. G., 1997: In-flight calibration of NOAA AVHRR visible and near-IR bands over Greenland and Antarctica. *Int. J. Remote Sens.,* **18,** 477–490.

Masonis, S. J., and S. G. Warren, 2001: Gain of the AVHRR visible channel as tracked using bidirectional reflectance of Antarctic and Greenland snow. *Int. J. Remote Sens.,* **22,** 1495–1520.

Mischenko, M. I., I. V. Geogdzhayev, B. Cairns, W. B. Rossow, and A. A. Lacis, 1999: Aerosol retrievals over the ocean by use of channels 1 and 2 AVHRR data: Sensitivity analysis and preliminary results. *Appl. Opt.,* **38,** 7325–7341.

Mitchell, R. M., 1999: Calibration status of the NOAA AVHRR solar reflectance channels: CalWatch Revision 1. CSIRO Atmospheric Research Tech. Paper 42, 20 pp.

Nakajima, T. Y., and T. Nakajima, 1995: Wide-area determination of cloud microphysical properties from AVHRR measurements for FIRE and ASTEX regions. *J. Atmos. Sci.,* **52,** 4043–4059.

Rao, C. R. N., and J. Chen, 1995: Inter-satellite calibration linkages for the visible and near-infrared channels of the Advanced Very High Resolution Radiometer on the *NOAA-7, -9,* and *-11* spacecraft. *Int. J. Remote Sens.,* **16,** 1931–1942.

——, and ——, 1996: Post-launch calibration of the visible and near-infrared channels of the Advanced Very High Resolution Radiometer on the *NOAA-14* spacecraft. *Int. J. Remote Sens.,* **17,** 2743–2747.

Stroeve, J., A. Nolin, and K. Steffen, 1997: Comparison of AVHRR-derived and in situ surface albedo over the Greenland ice sheet. *Remote Sens. Environ.,* **62,** 262–276.

Tahnk, W. R., and J. A. Coakley Jr., 2001a: Improved calibration coefficients for *NOAA-14* AVHRR visible and near-IR channels. *Int. J. Remote Sens.,* **22,** 1269–1283.

——, and ——, 2001b: Updated calibration coefficients for *NOAA-14* AVHRR channels 1 and 2. *Int. J. Remote Sens.,* **22,** 3053–3057.

Wetzel, M. A., and L. L. Stowe, 1999: Satellite-observed patterns in stratus microphysics, aerosol optical thickness, and shortwave radiative forcing. *J. Geophys. Res.,* **104,** 31 287–31 299.